Optimal Design of Double-Sided Linear Flux Switching Permanent Magnet Motor

Qiankai Zhao, Cheng Wen*, Xingqiao Zhao, Mingwei Li, Kailin Lv, and Xin Wang

Abstract—This paper studies the optimal design of a double-sided linear flux switching permanent magnet motor (DLFSPM) to improve the average thrust generated by motor operation and reduce the fluctuation range of thrust applying the Response surface methodology (RSM) and Particle Swarm Optimization (PSO). An analytical mathematical model of the electromagnetic thrust force of the DLFSPMs is developed. The functional model of the optimization parameters and objectives based on the RSM is constructed. The finite element analysis (FEA) is used to carry out numerical experiments on the geometric structure design variables. PSO is applied to an optimization tool for optimizing the DLFSPMs' mover structure parameters. Finally, the FEA comparison and analysis of the optimization results with the initial results reveal a significant improvement in the electromagnetic characteristics of the DLFSPMs. The feasibility and effectiveness of the optimization method are verified by the FEA results.

1. INTRODUCTION

Linear Motor (LM) has received extensive attention and applications in recent years because it does not require intermediate mechanical conversion devices such as mechanical gears. Compared with rotating motors, linear motors have a simpler structure, lower cost, better flexibility and dynamic performance [1, 2]. Permanent Magnet Linear Synchronous Motor (PMLSM), as its representative product, has the advantages of high efficiency, high-speed, high-power factor, etc., and it is widely used in traction drive, precision lathe, automatic production, and other fields. As a special permanent magnet linear motor, DLFSPMs has small axial force and large thrust density compared with traditional permanent magnet linear motor. Its development has attracted more and more attention from scholars and industry [3]. Refs. [4–6] proposed DLFSPMs for rail transit traction system, and thrust density and thrust fluctuation are its two important indicators. However, with the development of technology, the industry's requirements for these two indicators are getting higher.

In order to solve the above shortcomings in the optimization design of the motor and improve the efficiency of the solution, researchers now mostly introduce computer optimization algorithms into the optimization design of the motor. In [7], Wang et al. used GA for PMLSMs thrust optimization design. Compared to traditional optimal algorithms, GA is more responsive and more accurate, but tends to get stuck in local optimal solutions. Sun et al. introduced a multilevel optimization strategy for multi-objective optimization of IPMSM. They applied Pearson correlation coefficient analysis and cross-factor variance analysis techniques to evaluate the correlation between design parameters and optimization objectives, and approximated the FEA results by Krigingmodel [8]. In [9], researchers have used fuzzy method and sequential Taguchi method for the optimal design of IPMSM, while they introduced a fuzzy inference system to transform the multi-objective optimization problem into a single-objective optimization problem. These have achieved relatively good optimization results. Shi et

The authors are with the School of Electrical and Electronic, Shijiazhuang Tiedao University, Shijiazhuang 050043, China.

al. integrated Taguchi method, fuzzy theory, and sequential optimization strategy and proposed a fuzzy-based sequential Taguchi robust optimization method for the optimal design of five-phase permanent magnet motors in [10]. In [11], Pan and Fang used the random forest algorithm to train the parameters of the permanent magnet arc motor and then obtain the regression model. The advantages of this type of machine learning are quickly training speed and high degree of fit. But it requires a large amount of sampling point data, and the regression model is difficult to express using mathematical relationships.

This paper proposes an optimization method to improve the performance of DLFSPMs, which aims to further increase the thrust density of DLFSPMs and reduce the range of thrust fluctuations, while avoiding the shortcomings of existing methods. The application of this method combines Response Surface Method (RSM) and Particle Swarm Algorithm (PSO). RSM is used to construct the model to be optimized, and PSO is applied to solve the global optimal solution of the optimized model.

The structure of the article adopts the following arrangement. Section 2 introduces the initial motor topology and electrical characteristics of the DLFSPMs. In Section 3, the optimization of parameters is determined on the basis of the mathematical model, and the results are verified by FEA. In Section 4, the response surface model of this experiment is constructed and evaluated, and the design of the mover structure of DLFSPMs is optimized. The performances of the original and optimized DLFSPMs are compared through FEA, and some conclusions are provided in Section 5.

2. INITIAL STRUCTURE AND PARAMETERS OF DLFSPMS

2.1. Establishment of the DLFSPMs Model

The purpose of this study is to increase the average thrust and reduce the range of thrust fluctuations by designing and improving the structural parameters of the DLFSPMs. At the beginning of the design, the main structural parameters and electrical characteristics of the DLFSPM motor are defined. Fig. 1 shows the two-dimensional structure of the initial structure of DLFSPMs.

Figure 1 shows that the linear motor adopts a long secondary structure, and the length of the stator is greater than the length of the mover. The primary mover is composed of five double-H-shape and two H-shape magnetic cores. The PM are arranged between the conductor cores, and it is magnetized in the direction of motion of the motor [12]. We define the structural parameters of DLFSPM which are shown in Table 1.
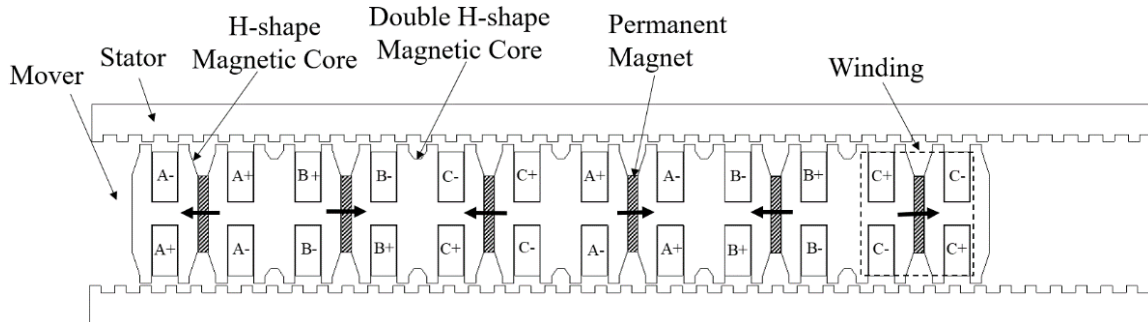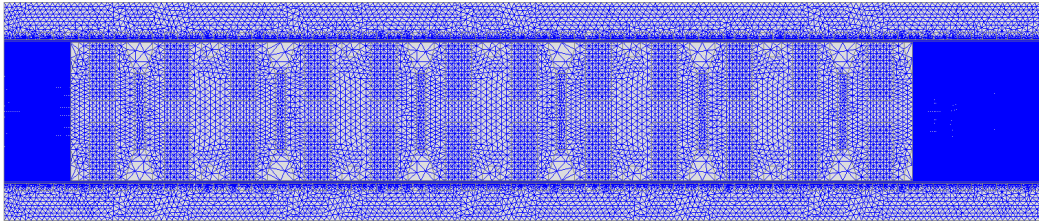

Figure 1. Initial model of DLFSPMs.

Table 1. Structural parameters of initial model.

| Parameter (mm)	Value	Parameter (mm)	Value
Stator pole pitch	9.9	Stator tooth width	4.455
Stator tooth height	2.1	Stator yoke	11
Mover tooth width	4.455	Mover tooth height	2.8
Mover yoke	9	Mover pole pitch	14.85
PM length	4	Air gap	1

2.2. Electromagnetic Performance of the Initial Model

As a widely accepted method for modeling electric motors, FEA simulates a real motor system by using mathematical approximations. It divides the motor model into a finite number of simple and interacting elements, which enables the approximation of a real system with a finite number of units to an infinite number of unknown quantities. In this paper, the FEA mesh structure of DLFSPM is shown in Fig. 2. Using FEA software to simulate the initial model of the DLFSPM motor, the following results are obtained:

Figure 2. The mush structure of DLFSPMs.

(1) Figure 3 shows the simulation results of no-load back-EMF. The FEA results for the no-load EMF are illustrated in Fig. 3(a). The three-phase no-load EMF amplitudes of the DLFSPMs initial model are $V_{A\,\max} = 17.01\,\text{V}$, $V_{B\,\max} = 18.37\,\text{V}$, and $V_{C\,\max} = 16.75\,\text{V}$. Fig. 3(b) shows the harmonic distortion rate of the electromotive force of the A-phase winding, and the horizontal axis represents the harmonic order. The third harmonic has the greatest impact, and its harmonic distortion rate is 6.82%. The total harmonic distortion (THD) rate is 7.27%.
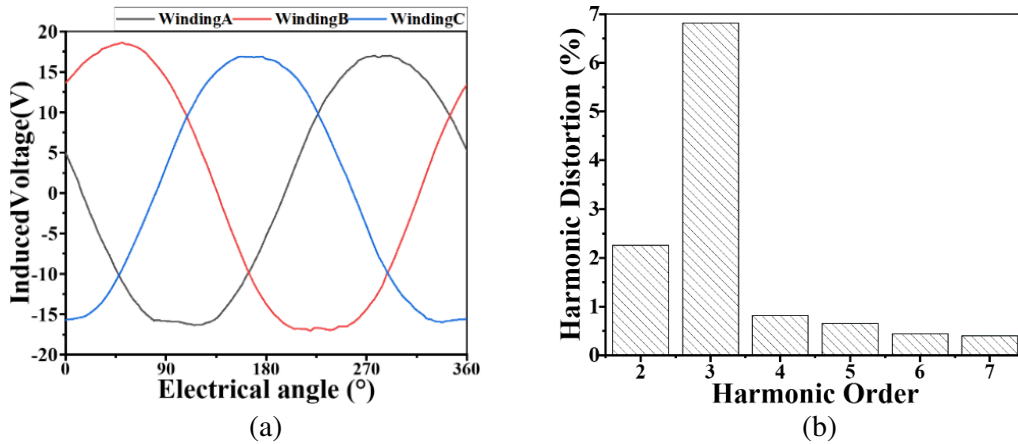

Figure 3. The simulation results of EMF of no-load.

(2) The magnetic density cloud of the initial model of DLFSPMs is shown in Fig. 4(a). The magnetic density is distributed in the range of $0 \sim 2.3$ Tesla. The brighter the color is, the more serious the magnetic saturation is. Fig. 4(a) shows that the magnetic saturation can be found in three positions: the mover yoke, mover teeth, and stator teeth. This will cause the core of the mover to heat up and reduce the service life of the motor.

(3) The simulated thrust waveform is shown in Fig. 4(b). The average thrust of the initial model of DLFSPMs is 385.37 Newton. In addition, the thrust fluctuation coefficient (F_{rip}) reflects the fluctuation of thrust:

$$F_{rip} = \sqrt{\frac{F_{\max} - F_{\min}}{F_{avg}}} \tag{1}$$
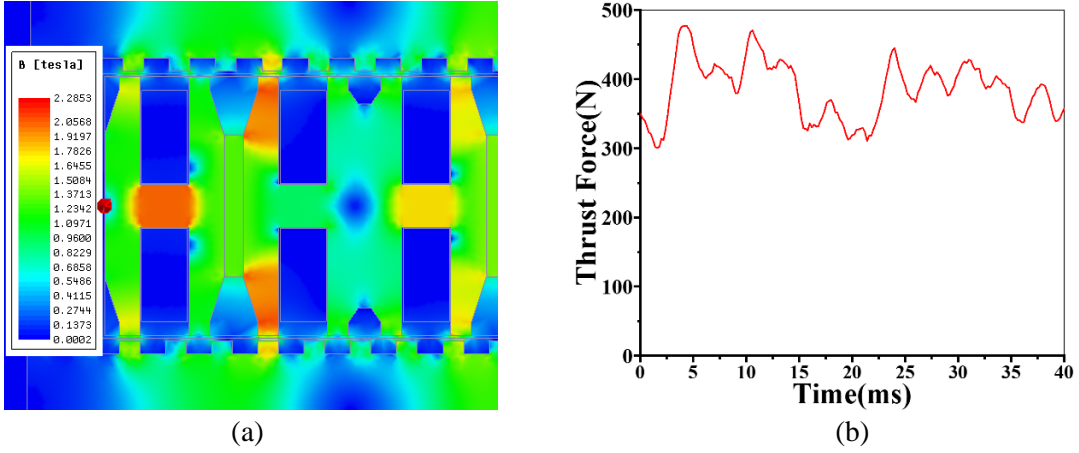
Figure 4. Characteristics of the primary DLFSPMs. (a) The magnetic density cloud of the initial model. (b) Thrust simulation results of the initial model.

The thrust fluctuation coefficient of the initial model calculated from Eq. (1) is $F_{rip} = 0.6768$. F_{avg} and F_{rip} of the initial model cannot meet the requirements of the traction drive field.

Based on the above analysis, it is necessary to optimize the structural parameters of the initial model for DLFSPMs.

3. PARAMETER SELECTION BASED ON ANALYSIS MODEL

The work to be accomplished in this section is to determine the parameters to be optimized with the mathematical model of the DLFSPMs thrust. First of all, the following assumptions are effective here [12, 13]:

1) Assume that the permeability of the core is infinite.
2) The relative permeability of permanent magnets will not change.
3) The magnetic field changes only in the direction perpendicular to motor operation.
4) Ignore the magnetic flux leakage of the air gap.

Based on above assumptions, the thrust of DLFSPMs (F) can be expressed as:

$$F = F_{em} + F_{cog} = F_{PM} + F_r + F_{cog} \tag{2}$$

where F_{PM}, F_r, F_{cog} represent the permanent magnet thrust component, reluctance thrust component, and detent force. They can be expressed as:

$$F_r = \frac{1}{2}I^T \cdot \left(\frac{d}{dx}L\right) \cdot I \tag{3}$$

$$F_{PM} = \frac{d}{dx}\left(\Psi_{PM}^T \cdot I\right) = N_{ph}I \cdot \frac{d\phi_m}{dx} \tag{4}$$

$$F_{cog} = -\frac{1}{2}\phi_m^2 \cdot \frac{dR_g}{dx} \tag{5}$$

where I represents the armature current, and its amplitude is I_m. The length of magnetic circuit is expressed in terms of L. ϕ_m represents the air gap flux. Air gap magnetoresistance is represented by R_g. x represents the displacement of the motor mover. Eq. (4) can continue to expand as:

$$F_{PM} = \frac{d\Psi_{PMa}}{dx} \cdot i_a + \frac{d\Psi_{PMb}}{dx} \cdot i_b + \frac{d\Psi_{PMc}}{dx} \cdot i_c = \frac{3}{2} \cdot \frac{2\pi}{\tau_\rho}\Psi_m I_m \cdot \cos\alpha \tag{6}$$

where Ψ_m is the amplitude of the flux linkage of each phase winding. α represents the phase difference between the armature current and the EMF. Combining formulas $(3) \sim (5)$ can be expressed as:

$$F = \frac{1}{2} I^T \left(\frac{d}{dx} L \right) I + N_{ph} I \cdot \frac{d\phi_m}{dx} - \frac{1}{2} \phi_m \frac{dR_g}{dx} \qquad (7)$$

According to the relationship among magnetomotive force, magnetic density, and magnetoresistance, the thrust of DLFSPMs can be changed by changing the magnetomotive force and magnetoresistance of each part.

Figure 5 shows a part of the mover's 3-D structure of the initial model of DLFSPMs. According to the above analysis, changing the parameter values of mover tooth width (H_{st1}), permanent magnet magnetization length (L_{PM}), mover tooth height (L_{st3}), and mover yoke width (L_{sy}) will cause the thrust of the DLFSPM motor to change.
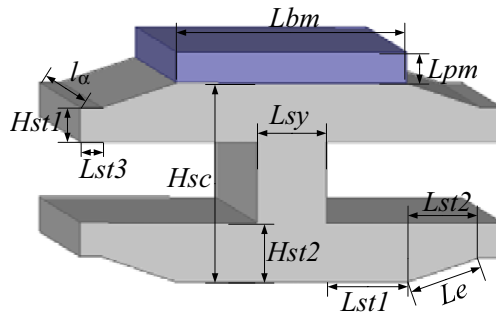

Figure 5. 3-D structure of part of the mover in the initial model of DLFSPMs.

We apply FEA to calculate F_{avg} and F_{rip} for different DLFSPMs operating conditions as shown in Fig. 6. It depicts the trends and conflicts between the two optimization objectives, which lays the foundation for the later multi-objective optimization.
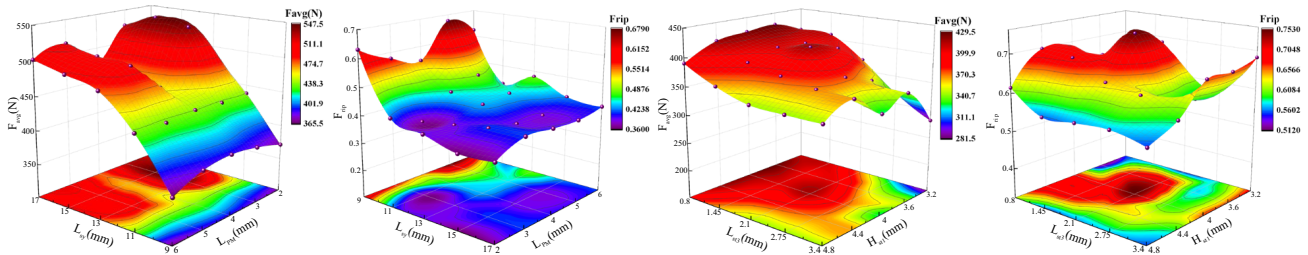

Figure 6. Variation of optimization objective with design variables.

4. STRUCTURAL PARAMETERS OPTIMIZATION OF DLFSPM

In this paper, the parameters of DLFSPMs mover structure are optimized by associating PSO and RSM. To define the objective function, this is the aim of RSM. As for the PSO, it is used to determine the optimal solution.

4.1. Construct the Objective Function

First, the objective function is completely established by RSM. It is often used for statistical application work. Its principle is: to find the relationship between the response and design variables, and establish a response surface model between them [14].

Before using RSM, determining the response and design variables is necessary. Define the response y_1 and y_2 as the average thrust (F_{avg}) and thrust fluctuation coefficient (F_{rip}) of DLFSPMs, respectively. Define the design variables x_i ($i = 1, 2, 3, 4$) as H_{st1} L_{PM} L_{st3} L_{sy}, respectively. The level value of each variable is shown in Table 2. Each design variable has three levels. Level -1, 0 and 1 are defined as the minimum, average, and maximum values of the parameters in this paper, respectively.

Table 2. Parameter level.

Level	Design Variable (mm)			
	x_1	x_2	x_3	x_4
1	3.4	2	0.8	9
	4.1	3.5	1.8	13
1	4.8	5	2.8	17

We use the Central Composite Design (CCD) to build the sample distribution [12], and FEA is applied to calculate the results of each set of samples. The total number of samples is 31, and a summary of the results can be found in Table 3.

Table 3. The results of sample distribution and FEA.

EXP.	x_1	x_2	x_3	x_4	F_{avg}	F_{rip}
1	3.2	2	0.8	9	465.224	0.619
2	4.8	2	0.8	9	417.588	0.664
...	...	...	...	...	...	...
3	3.4	3.5	1.8	13	450.646	0.537
31	4.8	3.5	1.8	13	503.559	0.685

After getting the sample data, using RSM to construct objective function. The relationship between design variable (x_i) and response (y_i) can be expressed as:

$$\begin{cases} y_1 = f_1(x_i) \\ y_2 = f_2(x_i) \end{cases} \quad (i = 1, 2, 3, 4) \tag{8}$$

In the classic RSM, the form of quadratic polynomial is usually selected as the response model:

$$y = \beta_0 + \sum_{i=1}^{n} \beta_i x_i + \sum_{i=1}^{n} \sum_{j=1}^{n} \beta_{ij} x_i x_j + \varepsilon \tag{9}$$

where x, β, and ε represent design variables, regression coefficients, and random errors, respectively. Express Eq. (9) in matrix form:

$$Y = X\beta \tag{10}$$

where $X = [1, x_1, \ldots, x_k, x_1^2, \ldots, x_k^2, x_1 x_2, x_1 x_3, \ldots, x_{k-1} x_k]$. β is calculated according to the least square method [15]:

$$\beta = \left(X^T X\right)^{-1} X^T Y \tag{11}$$

where Y is the matrix of response. X^T is the transposed matrix of X.

According to Table 3 and Equations (8) $\sim$ (11), the objective function of the DLFSPMs to be optimized can be obtained:

$$\begin{aligned} y_1 = & -491.2085 + 364.7574x_1 + 29.7377x_2 - 53.0676x_3 - 34.5124x_4 \\ & -62.3067x_1^2 - 24.1607x_2^2 + 6.3191x_3^2 - 2.197x_4^2 + 18.802x_1 x_2 \\ & +10.582x_1 x_3 + 5.95x_1 x_4 - 8.497x_2 x_3 + 3.352x_2 x_4 - 0.86x_3 x_4 \end{aligned} \tag{12}$$

$$\begin{aligned}
y_2 = {} & -0.9981 + 1.1896x_1 + 0.0476x_2 + 0.0324x_3 - 0.1265x_4 \\
& -0.1383x_1^2 + 0.0245x_2^2 - 0.0255x_3^2 + 0.004x_4^2 - 0.0171x_1x_2 \\
& +0.007x_1x_3 + 0.012x_1x_4 + 0.0152x_2x_3 - 0.0004x_3x_4
\end{aligned} \tag{13}$$

4.2. Evaluation of Regression Results

After obtaining the functional relationship between the response and design variables, it is necessary to evaluate the regression result of the objective function. The decision coefficient R^2 is given by:

$$R^2 = 1 - \frac{\displaystyle\sum_{i=1}^{n}(y_i - \hat{y}_i)^2}{\displaystyle\sum_{i=1}^{n}(y_i - \bar{y}_i)^2} \tag{14}$$

where y_i, $\bar{y}_i$, and $\hat{y}_i$ respectively represent the true, average value, and predicted results of the test data. According to Eq. (14), the decision coefficients of Eqs. (12) $\sim$ (13) are $R_1^2 = 99.05\%$ and $R_2^2 = 98.12\%$.

Figure 7 purposes the comparison of the true and predicted distributions of the average thrust and thrust fluctuation coefficient of the data in Table 4. The results of FEA coincide well with the predicted results of RSM. Therefore, the objective functions (12) $\sim$ (13) have the characteristics of high sensitivity and good fitting accuracy, which meet the requirements of this optimization design.
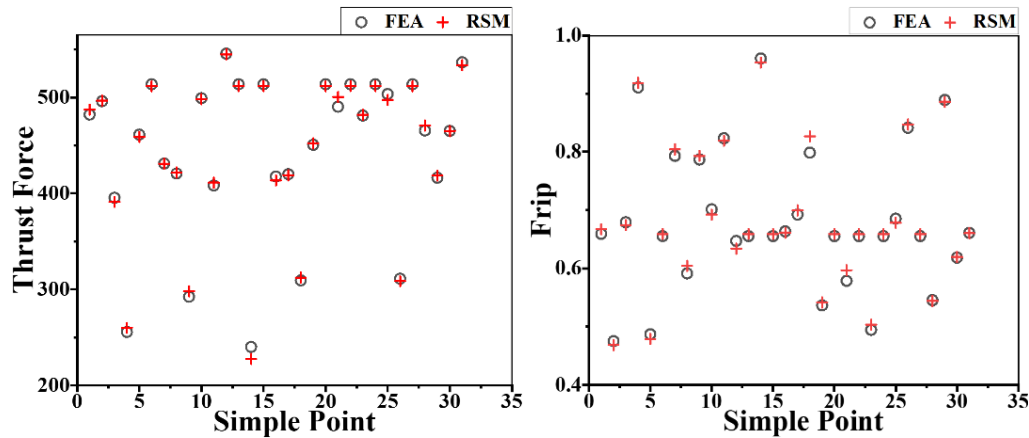

Figure 7. Distribution of true and estimated values.

Table 4. Parameters of PSO.

Parameter	Value
Particle population	20
$\omega_{\max}$	0.9
$\omega_{\min}$	0.4
Acceleration factor (c_1, c_2)	2
$T_{\max}$	500

4.3. The Process of Optimization

The details of PSO can be found in [16]. Due to its simplicity and controllability, PSO has been widely applied to solve target optimization problems [17]. The parameters of PSO are shown in Table 4. We apply the PSO toolbox of MATLAB software to perform iterative calculations.

In addition, PSO has a powerful single-objective optimization performance, so it is necessary to introduce weight coefficients to improve the objective function. Here, the value of the weight coefficient is 0.5. According to Eqs. (12) $\sim$ (13), the new objective function can be defined as:

$$Y = -0.5y_1 + 0.5y_2 \tag{15}$$

PSO stops running after 500 iterations. Fig. 8 shows the results of PSO operation. The results show that PSO obtains the global optimal solution after 14 iterations of calculation. The optimal solution is:

$$\begin{cases} H_{st1} = 4.13\,\text{mm} & L_{PM} = 2.97\,\text{mm} \\ L_{st3} = 1.51\,\text{mm} & L_{sy} = 16.03\,\text{mm} \end{cases} \tag{16}$$
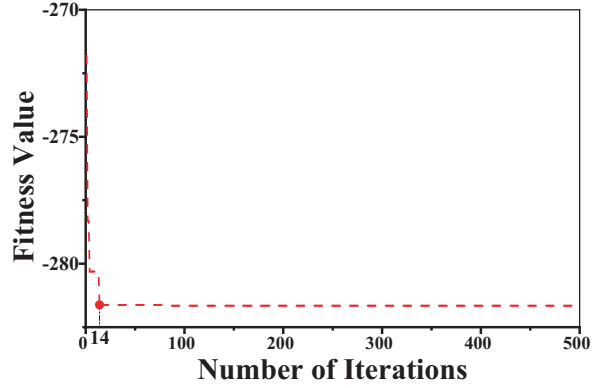

Figure 8. The result of PSO.

4.4. Optimization Results

We take the obtained Eq. (16) into the DLFSPMs model for FEA calculation and obtain the following optimization results:

(1) The FEA results about no-load back-EMF after optimization are purposed in Fig. 9(a). The amplitude of the no-load back EMF after optimization is increased by about 61.1% compared with Fig. 3(a).

(2) The comparison result of initial and optimal models about the harmonic distortion rate of the A-phase winding no-load back EMF is illustrated in Fig. 9(b). Comparing Fig. 9(b) with Fig. 3(b),
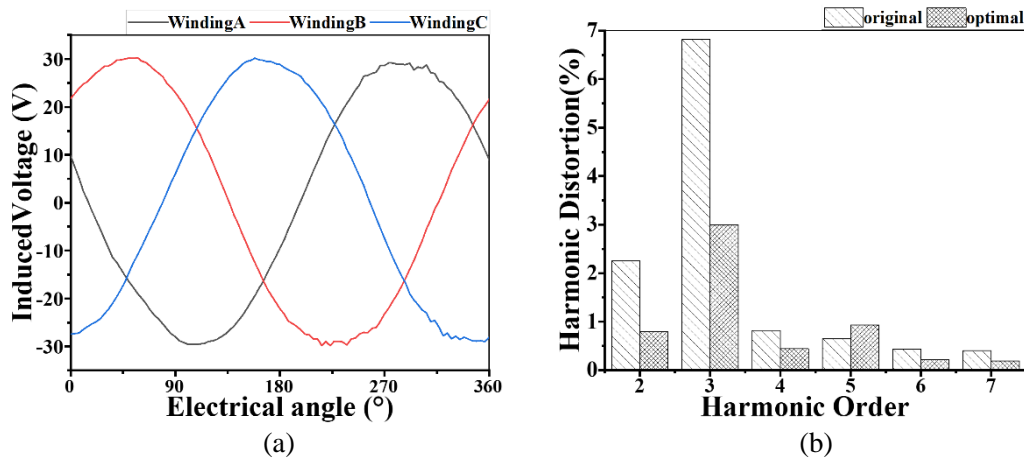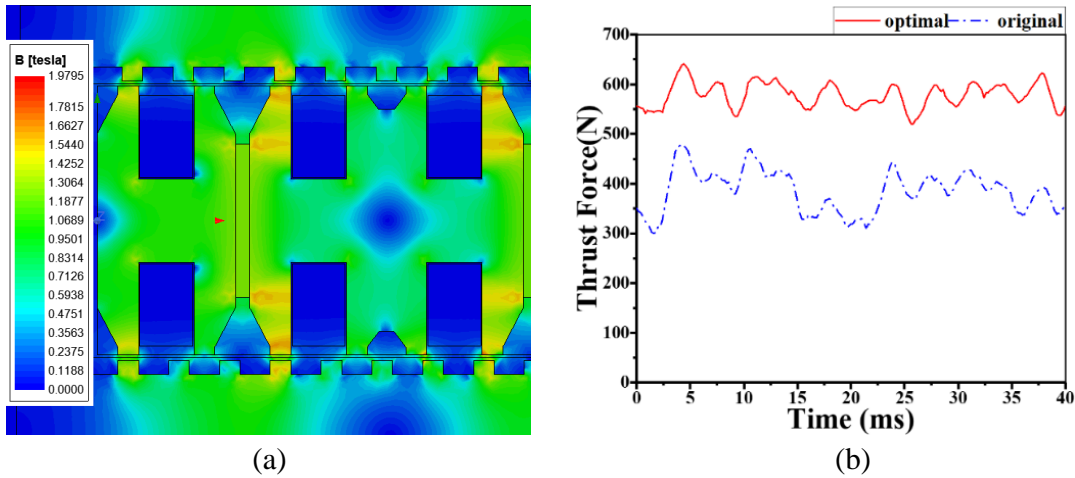

(a)   (b)

Figure 9. No-load back-EMF of optimized DLFSPMs. (a) Waveform of three-phase. (b) Comparison chart of harmonic analysis between initial and optimized models.

Figure 10. Characteristics of optimized DLFSPMs. (a) The density cloud map. (b) Comparison of thrust of the initial and the optimized model.

the influence of the 3rd harmonic is reduced after optimization, and it is reduced to 2.99%. The total harmonic distortion (THD) is reduced to 3.28%.

(3) Figure 10(a) shows the optimized DLFSPMs magnetic density cloud map. Compared with Fig. 4(a), it can be seen that the magnetic saturation phenomenon at the mover yoke, mover teeth, and stator teeth has been greatly improved. The magnetic density is distributed in the range of $0 \sim 1.98$ Tesla. This will make the motor run more stable.

(4) The comparison result of thrust is purposed in Fig. 10(b). The average thrust of the optimized model is 570.587 Newton. The thrust fluctuation coefficient is reduced to 0.4125. Through RSM-PSO parameter optimization calculation, the average thrust value of DLFSPMs is 48.06% higher than the initial model, and the thrust fluctuation of DLFSPM is reduced by 36.09% compared with the initial model.

5. CONCLUSION

This paper proposes a method to optimize the design of the mover structure of DLFSPMs by combining RSM and PSO. The average thrust of the motor is increased and the range of thrust fluctuations reduced. This article uses the RSM-based objective function building method. And decision coefficients are used to evaluate the regression degree of the objective function. The results show that the objective function fitted by RSM has the characteristics of high degree of fitting and perfect fitting accuracy. The feasibility of applying RSM to construct DLFSPMs optimization model is verified. In this paper, an optimal design of DLFSPMs with an approach combines PSO and RSM, and the optimization results are verified by FEA. No-load back-EMF peak value has been increased and THD reduced to 3.28%. The magnetic saturation phenomenon has been greatly improved. The motor runs more stably. In the end, the average thrust has been greatly improved, and the thrust fluctuation has become lower than before optimization. Therefore, the DLFSPMs optimization design method combining RSM and PSO can easily and effectively obtain the target optimal mover structure parameters.

ACKNOWLEDGMENT

REFERENCES

1. Liu, Y., X. Zhang, and S. Niu, "A permanent magnet linear motor with complementary flux and its optimization," *IEEE Transactions on Magnetics*, Vol. 55, No. 6, 1–5, June 2019.

2. Kwon, Y. and W. Kim, "Electromagnetic analysis and steady-state performance of double-sided flat linear motor using soft magnetic composite," *IEEE Transactions on Industrial Electronics*, Vol. 64, No. 3, 2178–2187, March 2017.

3. Lu, M. and R. Cao, "A novel double-sided high temperature superconducting linear modular flux-switching motor," *IEEE Transactions on Applied Superconductivity*, Vol. 31, No. 5, 1–10, August 2021.

4. Cao, R., M. Cheng, C. C. Mi, and W. Hua, "Influence of leading design parameters on the force performance of a complementary and modular linear flux-switching permanent-magnet motor," *IEEE Transactions on Industrial Electronics*, Vol. 61, No. 5, 2165–2175, May 2014.

5. Zhao, W., M. Cheng, J. Ji, R. Cao, Y. Du, and F. Li, "Design and analysis of a new fault-tolerant linear permanent-magnet motor for maglev transportation applications," *IEEE Transactions on Applied Superconductivity*, Vol. 22, No. 3, 5200204–5200204, June 2012.

6. Wu, J., X. Zhu, Z. Xiang, L. Xu, M. Jiang, and W. Pu, "Electromagnetic performance prediction of a double-rotor flux-switching motor based on general air-gap equivalent algorithms model," *2019 22nd International Conference on Electrical Machines and Systems (ICEMS)*, 1–6, Harbin, China, 2019.

7. Wang, X., J. Wu, R. Luo, and J. Li, "Design optimization of thrust density for permanent magnet linear motor based on genetic algorithm," *2018 IEEE 4th Information Technology and Mechatronics Engineering Conference (ITOEC)*, 1192–1198, Chongqing, China, 2018.

8. Sun, X., Z. Shi, and J. Zhu, "Multiobjective design optimization of an IPMSM for EVs based on fuzzy method and sequential taguchi method," *IEEE Transactions on Industrial Electronics*, Vol. 68, No. 11, 10592–10600, November 2021.

9. Sun, X., Z. Shi, G. Lei, Y. Guo, and J. Zhu, "Multi-objective design optimization of an IPMSM based on multilevel strategy," *IEEE Transactions on Industrial Electronics*, Vol. 68, No. 1, 139–148, January 2021.

10. Shi, Z., X. Sun, Y. Cai, and Z. Yang, "Robust design optimization of a five-phase PM hub motor for fault-tolerant operation based on taguchi method," *IEEE Transactions on Energy Conversion*, Vol. 35, No. 4, 2036–2044, December 2020.

11. Pan, Z. and S. Fang, "Combined random forest and NSGA-II for optimal design of permanent magnet arc motor," *IEEE Journal of Emerging and Selected Topics in Power Electronics*, 2021.

12. Liu, Q., et al., "Cogging force reduction of double-sided linear flux-switching permanent magnet machine for direct drives," *IEEE Transactions on Magnetics*, Vol. 49, No. 5, 2275–2278, May 2013.

13. Cheng, M., P. Han, and W. Hua, "General airgap field modulation theory for electrical machines," *IEEE Transactions on Industrial Electronics*, Vol. 64, No. 8, 6063–6074, August 2017.

14. Aun, T., N. M. Salleh, U. F. M. Ali, and N. S. A. Manan, "Optimization of a Cu-O-based sensor for the detection of glucose using a central composite design," *IEEE Sensors Journal*, Vol. 20, No. 20, 12109–12116, October 15, 2020.

15. Chan, K. S., S. J. Greaves, and S. Rahardja, "Techniques for addressing saddle points in the Response Surface Methodology (RSM)," *IEEE Access*, Vol. 7, 85613–85621, 2019.

16. Kennedy, J. and R. Eberhart, "Particle swarm optimization," *Proceedings of ICNN'95 — International Conference on Neural Networks*, Vol. 4, 1942–1948, Perth, WA, Australia, 1995.

17. Tang, G., J. Sheng, D. Wang, and S. Men, "Continuous estimation of human upper limb joint angles by using PSO-LSTM model," *IEEE Access*, Vol. 9, 17986–17997, 2021.